INTUITIVE REAL-TIME COMPENSATION ALGORITHM FOR ACTUATOR CONTROL ERRORS IN FAST PSEUDODYNAMIC TESTS

Ronald J. Gultom[1] and Quincy T. Ma[2]

SUMMARY

Time delay error is common in fast pseudodynamic (PSD) tests due to the effect of actuator dynamics. This type of systematic error introduces energy into a system which if not monitored or controlled, can result in test instability and cause the response to grow exponentially. This leads to premature termination of a simulation and unreliable results. This paper proposes an intuitive error-compensation algorithm to correct this error by considering the systematic error as negative damping in the system. The key to this scheme is the introduction of varying viscous damping at each integration time step during the PSD test. The magnitude of the time-varying viscous damping is derived by equating the magnitude of the energy error with that dissipated by the introduced damping at every integration time step. Numerical simulations and experimental validations are presented in this paper to illustrate the effectiveness of the algorithm, to produce reliable simulation results in the presence of systematic time delay error and noisy measurements.

INTRODUCTION

Pseudodynamic (PSD) testing is an evolving and popular laboratory based physical testing technique for simulating dynamic loads on structures. In a PSD test, a specimen is subjected to a displacement history that is determined interactively according to a numerical model of the system and the measured specimen response during the course of the test [1]. This testing technique is particularly advantageous for seismic simulations, as it allows dynamic and inertial effects to be replicated in the numerical model, hence allowing otherwise very large dynamic forces on the physical specimens to be applied at a slower rate or pseudo- statically.

PSD TEST METHOD

The PSD test method solves the time-discretized equation of motion of a structure subjected to external excitations. This can be formulated as,

$$\boldsymbol{M}\ddot{u}_i + \boldsymbol{C}\dot{u}_i + \boldsymbol{R}_i = \boldsymbol{F}_i \qquad (1)$$

where subscript i denotes a quantity at the i^{th} time step, $\boldsymbol{M}$ and $\boldsymbol{C}$ are the system's mass and viscous damping matrices respectively, $\boldsymbol{R}$ is the restoring forces vector, $\ddot{u}$ and $\dot{u}$ are the nodal acceleration and velocity vectors respectively, and $\boldsymbol{F}$ is the vector of external excitations. Should the external excitations arise as a result of a vector of ground accelerations $\ddot{u}_g$, $\boldsymbol{F}$ is equal to $-\boldsymbol{M\Gamma}\ddot{u}_g$ where $\boldsymbol{\Gamma}$ is the interaction matrix.

In a PSD test, the displacements of the system are determined in a stepwise fashion through numerical integration of Equation 1. As new displacements are determined, they are applied to the test specimen through actuators and the restoring forces of the system ($\boldsymbol{R}$) are experimentally measured and re-inserted into Equation 1 for evaluating the system displacements at the next time step. This process repeats until the desired response history is obtained. The advantages of this technique over conventional nonlinear numerical analyses and common cyclic pseudo-static tests are that 1) no assumption of the system's force-deformation relationship is required, 2) the loading history on the test specimen is not predetermined and closely emulates that expected during the excitation, 3) inertial effects can be numerically simulated to predict dynamic time history response. More detailed descriptions of the PSD test method can be found in the works by other researchers [2, 3].

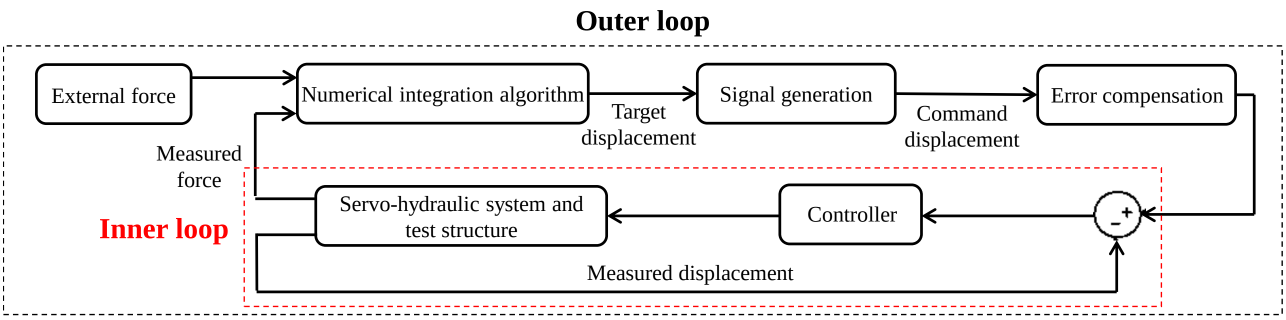

Figure 1: Block diagram of a fast PSD test

[1] PhD Candidate, Department of Civil and Environmental Engineering, The University of Auckland, Auckland

[2] Lecturer, Department of Civil and Environmental Engineering, The University of Auckland, Auckland

FAST PSD TEST

A weakness of the conventional PSD test is its inability to directly replicate strain-rate dependent effects. This is problematic when analysing structures with rate-sensitive behaviours, such as structures with viscoelastic dampers and base isolated systems. This led to the development of the fast PSD test method where the specimen is loaded at or near real-time [4]. One of the first fast PSD test was conducted by Nakashima *et al.* [5] on a single-degree-of-freedom (SDOF) system loaded by a single actuator. The method has since been adopted and refined by other researchers [6-9]. In the test conducted by Nakashima *et al.* [5], loading was applied via a dynamic actuator with the motion monitored at a sampling rate of 1 kHz. In addition to dynamically rated actuator, a fast PSD test also requires sophisticated computing hardware to enable high speed data communications between the computer solving the equation of motion and the actuator controller [9].

Figure 1 shows a block diagram of a fast PSD test. The state-of-the-art PSD test can be viewed as a dual loop system [10] consisting of an outer loop and an inner loop. The outer loop solves the equation of motion and determines the target displacement at each integration time step; meanwhile the inner loop generates the necessary analogue command from the controller to the servo-hydraulic hardware which guides the test structure to follow the commanded displacement from the outer loop, by comparing the last measured displacement of the test structure with the new target displacement at each experimental time step.

In a fast PSD test, the outer loop performs two additional tasks; 1) a “signal generation” task which synchronizes the integration and the experimental sample rate. An example is the extrapolation-interpolation method proposed by Nakashima and Masaoka [7]; and 2) an "error compensation" task which preconditions the command displacements to correct for anticipated errors in the inner loop process. Research has shown that this task has a significant effect on the stability and reliability of a fast PSD test.

ERRORS IN PSD TEST

The PSD test method is a reliable alternative to shake table tests provided errors are properly mitigated [11, 12]. There are two types of errors associated with PSD tests, numerical errors and experimental errors. Numerical errors arise from the computation process, for example from structural idealisation where a discrete-parameter system is used to approximate the actual continuous system. Inherent errors in the numerical integration process can also be significant when the parameters are not properly selected [13]. Numerical errors are inherent in every dynamic analysis procedure and cannot be completely eliminated from a PSD test [12]. Experimental errors arise from inaccurate laboratory equipment control or measurements during a simulation. Numerical errors often exacerbate the experimental errors and lead to unique error propagation characteristics. Experimental errors can be further classified into random and systematic errors. Random errors are irregular by nature and no specific effect on the solution can be anticipated. An example of random error source is electronic noise in measurement devices. Systematic errors in contrast are approximately regular and predictable. A list of some systematic errors sources can be found in Shing and Mahin [14]. This study also shows that systematic errors have a greater detrimental effect on the accuracy and the stability of the solution process when compared to random errors.

Systematic Displacement Control Error

One common and significant form of systematic errors is displacement control error. This occurs when the displacements applied to a specimen are systematically larger or smaller than the target displacements at the time when force measurements are required by the solution algorithm. This can occur via two mechanisms. Actuators can exhibit constant undershoot or overshoot errors, in which the actuators will move in phase with the command but always exceed or fall behind the command for the entire motion of the actuator. This commonly occurs to actuators under simple closed loop control and can be a result of mis-calibration, digitisation error, amongst other causes. Additionally, during fast or real time PSD tests, actuator movement will always lag the actuator command. Depending on the direction of loading and the tuning of the actuator control loop, this time delay lead to actuator undershooting or overshooting the command during different phases of loading. This type of error is characterised by a phase shift of the actuator movement against the command. Both of these systematic mechanisms affect the energy balance in the system and affect the PSD test results [14-17].

Energy Content in a Structural System and Displacement Control Errors

The change in mechanical energy content in a structural system is the sum of the work done by the inertial, dissipative and elastic restoring components. This balances with the work done by the external forces in lieu of any errors. This can be expressed mathematically as Equation 2, which is simply the governing equation of motion (Equation 1) integrated with respect to displacements. Equation 2 assumes the structural system is initially at rest and the system is elastic.

$$\int (\boldsymbol{M}\ddot{u})^T\ du + \int (\boldsymbol{C}\dot{u})^T\ du + \int \boldsymbol{R}^T\ du = \int \boldsymbol{F}^T\ du \quad (2)$$

The third term in Equation 2 represents the strain energy content. In a PSD test, this quantity depends on the measured restoring force from the test specimen. Any displacement control errors will result in erroneous displacements and hence erroneous measured restoring forces. This in turns distorts the energy balance in the system described by Equation 2. The perceived energy content is expressed mathematically as,

$$\int (\boldsymbol{M}\ddot{u})^T\ du + \int (\boldsymbol{C}\dot{u})^T\ du + \int (\boldsymbol{R}^m)^T\ du = \int \boldsymbol{F}^T\ du \quad (3)$$

$$\boldsymbol{R}^m = \boldsymbol{R}^c + \boldsymbol{R}^{er} \quad (4)$$

In Equation 3 and 4, $\boldsymbol{R}^m$ is the restoring force vector measured from the specimen, $\boldsymbol{R}^c$ is the restoring force vector at the same time step had the displacements been correctly applied, and $\boldsymbol{R}^{er}$ are the restoring force errors due to the displacement control errors. The energy error across a time-step, $\boldsymbol{E}^{er}$, is thus,

$$\boldsymbol{E}^{er} = \int (\boldsymbol{R}^{er})^T du \quad (5)$$

Note equation 5 is a simplified version of the formula proposed by other researchers [16-18].

In a PSD test, the numerical integration algorithm calculates the time history response using the measured restoring forces from the test specimen and commanded (computed) displacements. This leads to an interesting conundrum as the command and measured displacements are not necessarily the same due to the presence of errors. Consequently the measured restoring force is not a corresponding quantity to the commanded displacement. Consider a linear-elastic structure tested pseudodynamically, Figure 2 shows a perceived force-deformation relationship of a linear-elastic structure where consistent displacement control errors are present. The behaviour of the test structure as observed by the integration algorithm can be thought as a vertical departure of the restoring forces from the true linear elastic response. As the restoring force errors are proportional to the incremental displacements, and as incremental displacements approximate system velocities, these errors have similar effects as viscous damping. In the case of consistent time delay depicted in Figure 2a, the measured force lags the command displacement. This leads to a perceived counter-clockwise hysteretic response. This behaviour adds energy into the test specimen, represented by the shaded area of the plot. Conversely, Figure 2b depicts the perceived response under consistent time lead. In this case, the perceived clockwise hysteretic response represents additional energy dissipation from the system [16]. Time delay errors are more common in fast PSD tests due to the dynamic interactions between the structure and the test apparatus (servo controller, servo valve and the hydraulic actuator). Owing to these interactions, a time delay exists between when the displacement is commanded and when the structure actually reaches the target displacement.

EXISTING DELAY COMPENSATION PROCEDURES

The time delay caused by dynamic interactions between the specimen and the actuator-controller system has been a subject of extensive investigations. Horiuchi *et al.* [19] was the first to establish that the effect of the time delay is equivalent to introducing negative damping to the system. It was also found that test instability could arise if the negative damping from the delay exceeds the system's inherent damping. This section summarises various methods that have been proposed to negate the effect of the involuntary time delay and thus mitigate the negative damping effect.

The existing delay compensation methods are largely based on predicting the response of the specimen based on known information of the specimen in previous time steps. Horiuchi *et al.* [19] proposed the use of simple polynomial extrapolation to predict displacement several time steps ahead to account for the delay, based on computed displacements at the current and several previous time steps. The term time step here referred to the size of time step employed in the direct integration method. It was found that a third order Lagrangian polynomial prediction yielded the optimum result in term of accuracy and stability. Darby *et al.* [20] found that a constant time delay such as that adopted by Horiuchi *et al.* [19] may not give satisfactory results if there was a large variation in the time delay, particularly important when the structure undergoes inelastic deformations. Consequently, Darby proposed a method to estimate the delay interactively during a PSD experiment. Carrion and Spencer [21] developed a model based prediction that incorporated known information about the structure, including the inertial and damping characteristics, an estimate of the restoring force behaviour and the external excitation. This method allowed a longer prediction horizon in cases of longer time delay when compared to the polynomial extrapolation method. Ahmadizadeh *et al.* [22] proposed a technique to estimate actuator time delay using polynomial fit of desired and measured displacement data points. In addition to modifying command displacements to account for actuator delay, the measured restoring force was also compensated by seeking the time when the desired displacement was achieved using a polynomial fitting technique.

More complex actuator delay compensation methods also exist. These generally required a transfer function for the controller-actuator-specimen system to be evaluated in the frequency domain. Zhao *et al.* [23] employed a first-order phase lead method to adjust the command displacement and generated restoring force for a total time delay in excess of 81 ms. Bonnet et al. [24] adopted a similar phase lead procedure in the minimal control synthesis with modified demand (MCSmd) outer loop controller implemented over a proprietary proportional-integral-derivative (PID) inner loop controller. Carrion *et al.* [25] adopted a feedforward-feedback compensation procedure as the outer loop controller while treating the inner loop as a plant controlled by the outer loop. Wallace *et al.* [26] utilised adaptive parameters to minimise the error in estimating the magnitude of time delay, analogous to the method proposed by Darby *et al.* [20] and to control the magnitude of the forward prediction. These adaptive parameters are intended to accommodate the possibility of large variations in dynamic responses of the test specimen. Likewise, Chen and Ricles [27] also incorporated adaptive parameters in a delay compensation method utilising the inverse of a simplified actuator delay model to minimise delay estimation error.

This study presents an error compensation technique that does not require actuator motion prediction or system transfer function identification. Instead of improving actuator tracking by forecasting the actuator motion and thus minimising the energy error, the proposed technique simply corrects the effect of actuator displacement errors in the numerical integration at every time step after they occur, by introducing additional damping and exploiting the properties of the errors.

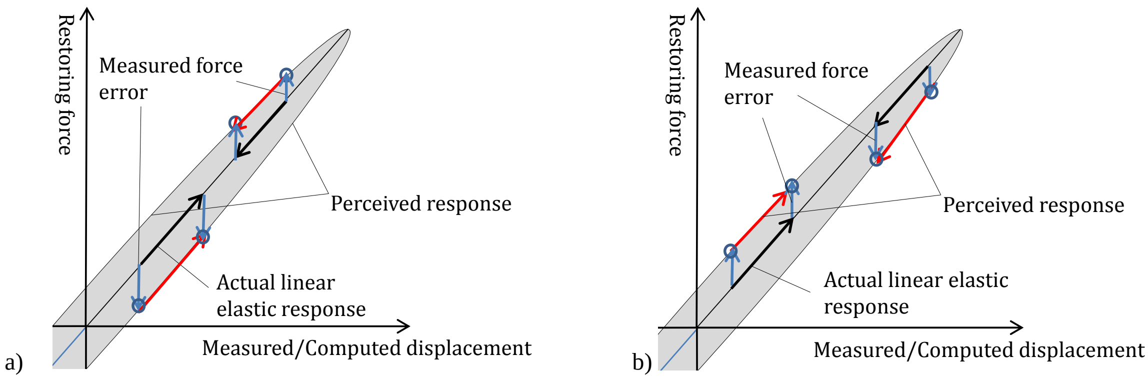

Figure 2: ***Idealised force-deformation response of system with displacement control errors under, a) time delay error, and b) time lead error [16].***

COMPUTATION OF ENERGY ERROR

The amount of energy error across a time step during a PSD test is approximately equal to the quadrilateral area between the true and perceived force-displacement response over the width of a displacement increment [15]. This energy error can be estimated using the trapezoidal rule as,

$$\boldsymbol{E}_i^{er} = \frac{1}{2}(\boldsymbol{K}_{i-1}u_{i-1}^{er} + \boldsymbol{K}_i u_i^{er})^T \Delta u_i^c \quad (6)$$

where subscript i denotes quantity at the i^{th} time step, $\boldsymbol{K}$ is the tangent stiffness matrix, u^{er} is the displacement errors at a time step given by $u^{er} = u^m - u^c$, where superscript m and c denote measured and ideal quantities respectively; and Δu_i^c is the target incremental displacements across a time step given by $\Delta u_i^c = u_i^c - u_{i-1}^c$.

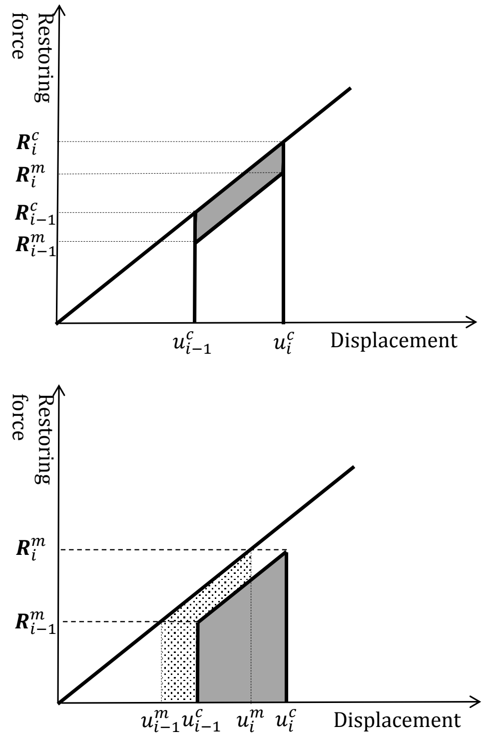

Figure 3: ***Displacement control error and the associated energy error according to a) Thewalt and Roman [15] and b) Mosqueda et al. [16].***

A drawback of this process is that it requires an estimate of the tangent stiffness of the system. This could be overcome by employing the measured forces and displacements from the specimen directly. The energy error across i^{th} time step ($\boldsymbol{E}_i^{er}$) is the difference in the change in strain energy as perceived by the numerical integration ($\boldsymbol{E}_i^{E}$) and in reality ($\boldsymbol{E}_i^{BE}$).

$$\boldsymbol{E}_i^{er} = \boldsymbol{E}_i^{BE} - \boldsymbol{E}_i^{E} \quad (7)$$

Equations 8 and 9 present the description for $\boldsymbol{E}_i^{E}$ and $\boldsymbol{E}_i^{BE}$ respectively.

$$\boldsymbol{E}_i^{E} = \frac{1}{2}(\boldsymbol{R}_{i-1}^m + \boldsymbol{R}_i^m)^T(u_i^c - u_{i-1}^c) \quad (8)$$

$$\boldsymbol{E}_i^{BE} = \frac{1}{2}(\boldsymbol{R}_{i-1}^m + \boldsymbol{R}_i^m)^T(u_i^m - u_{i-1}^m) \quad (9)$$

The above expressions provide a means to monitor in real time the accumulation of energy error in a PSD test [16]. These are the central equations for an error monitoring scheme called Hybrid Simulation Error Monitoring (HSEM). This scheme provides a timely warning when the accumulation of energy error in a PSD test exceeds a certain threshold, when the final result of the test would no longer be reliable and the test should be terminated, or continued only after corrective measures have been taken [16, 17]. The simplicity of the HSEM method is evident as it requires only quantities that are readily available at every time step during a fast PSD test.

Modification in Energy Error Computation

Due to the difference between the commanded incremental displacements (Δu^c) and the measured incremental displacements (Δu^m), the computations of energy error described in Equations 7 to 9 are modified. Consider a linear elastic structure with a force-deformation relationship as shown in Figure 3.

The energy error as computed by Equation 6 is highlighted by the bold area in Figure 3a. While the energy error as computed by Equation 7 is the difference in areas between the bold and dotted trapezoid.

The energy error calculated using Equation 7 is an approximate of the true energy error represented in Figure 3a. Despite the inexact nature, it is a more practical measure as it does not require knowledge of the instantaneous stiffness of the system.

For this investigation, it is further proposed that displacements are integrated with respect to the restoring force instead of the opposite for the energy error calculation. Adopting this modification, Equations 7 to 9 are now expressed as,

$$\boldsymbol{E}_i^{E\prime} = \frac{1}{2}(u_{i-1}^c + u_i^c)^T(\boldsymbol{R}_i^m - \boldsymbol{R}_{i-1}^m) \quad (10)$$

$$\boldsymbol{E}_i^{BE\prime} = \frac{1}{2}(u_{i-1}^m + u_i^m)^T(\boldsymbol{R}_i^m - \boldsymbol{R}_{i-1}^m) \quad (11)$$

$$\boldsymbol{E}_i^{er\prime} = \boldsymbol{E}_i^{BE\prime} - \boldsymbol{E}_i^{E\prime} \quad (12)$$

This modification in calculating energy error can be perceived as using complementary quadrilateral areas and are analogous with the actuator tracking indicator calculation adopted by Chen and Ricles [27]. A graphical explanation of Equations 10 and 11 is depicted in Figure 4.

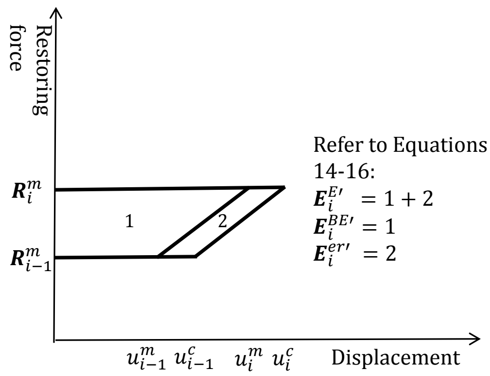

Figure 4: ***Graphical illustration of the energy error calculation outlined in Equations 10 to 12.***

Proposed Error Compensation Algorithm Utilising Artificial Viscous Damping

The HSEM method alone does not provide a means of correcting the error during simulation. The proposed scheme complements the HSEM method to intuitively compensate for errors interactively during a simulation, at or near real-time. This is achieved by introducing a variable amount of artificial viscous damping proportional to the energy error at each time step.

The amount of energy dissipated by viscous damping mechanism is given by the second term on the left-hand side of Equation 3. Using the trapezoid rule, this integration can be approximated as,

$$\boldsymbol{E}_i^D = \frac{1}{2}(\boldsymbol{C}\dot{u}_{i-1} + \boldsymbol{C}\dot{u}_i)^T(u_i^c - u_{i-1}^c) \tag{13}$$

where $\boldsymbol{E}_i^D$ is the energy dissipated through viscous damping across the i^{th} time step. It is assumed that the viscous damping matrix $\boldsymbol{C}$ is constant throughout the simulation. For clarity, this constant viscous damping is called the initial viscous damping matrix. The variable viscous damping matrix, represented by a new variable $\boldsymbol{C}_i^{cor}$, compensates for energy error $\boldsymbol{E}_i^{er}$ across the same step and can thus be derived by substituting $\boldsymbol{E}_i^{er}$ as $\boldsymbol{E}_i^D$ into Equation 13. This yields,

$$\boldsymbol{C}_i^{cor} = \frac{-2\boldsymbol{E}_i^{er}}{(\dot{u}_{i-1} + \dot{u}_i)(u_i^c + u_{i-1}^c)} \tag{14}$$

Incorporating this into Equation 3, the energy balance becomes,

$$\int(\boldsymbol{M}\ddot{u})^T du + \int(\boldsymbol{C}\dot{u})^T du + \int(\boldsymbol{R}^m)^T du + \int(\boldsymbol{C}_i^{cor}\dot{u})^T du = \int \boldsymbol{F}^T du \tag{15}$$

The term $\int(\boldsymbol{C}_i^{cor}\dot{u})^T du$ in Equation 15 compensates the energy error defined by Equation 5, which is inherent in the vector of restoring forces $\boldsymbol{R}^m$ (Equation 4)

Two important features to note,

1. The negative sign preceding $\boldsymbol{E}_i^{er}$ in Equation 14 indicates that the amount of additional viscous damping to compensate the energy error across a time step is the opposite amount introduced into the system due to the energy error.

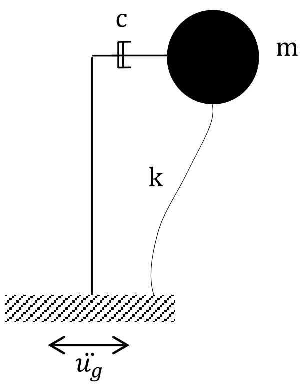

Figure 5: SDOF structure.

   For instance, if the energy error across a time step introduces negative damping
   into the structure, then the additional viscous damping $\boldsymbol{C}_i^{cor}$ is a positive definite matrix.

2. When an explicit numerical integration method such as the explicit Newmark method is used to solve the equation of motion, the velocity at the current time step $\dot{u}_i$ can not be determined before the equation of motion has been solved. In order to solve Equation 14 without iteration, the current velocity $\dot{u}_i$ in Equation 14 is replaced by the predictor velocity $\tilde{\dot{u}}_i$ which is expressed as

$$\tilde{\dot{u}}_i = \dot{u}_{i-1} + \Delta t\ddot{u}_{i-1} \tag{16}$$

NUMERICAL VERIFICATION

This section presents a number of numerical simulations for the purpose of confirming the validity and demonstrating the simplicity of the proposed compensation algorithm, for fast PSD tests with systematic errors. A linear elastic SDOF structure as shown in the Figure 5, are subjected to recorded earthquake excitations. The structure has dynamic properties as listed in Table 1. To study the sole effect of displacement control errors, other common sources of errors in a PSD test, for examples systematic truncation errors in digital to analogue (D/A) and analogue to digital (A/D) conversions, random electronic noises and mis-calibration in transducers are not simulated at this stage.

It should be noted that since the main purpose of this paper is to demonstrate the simplicity of the proposed scheme, the behaviour of the structure is limited to be as simple as possible, that is without the consideration of yielding, softening, or deterioriation, among others, that can occur.

A block diagram describing simulation process is shown in Figure 6. The "Integrator" block in Figure 6a conducts the numerical integration process using an explicit Newmark integration scheme, and the "Experimental specimen" block returns the ideal restoring force of a specimen using a simulated stiffness, representing a test specimen in the laboratory.

Table 1: SDOF structure properties

Dynamic properties	
Mass (kg)	1000
Stiffness (kN/m)	158
Damping ratio	0.02
Natural period (sec)	0.5

The "Simulated error" block modifies the command signal from the "Integrator" to emulate systematic actuator delays. This is achieved by introducing a normally distributed random multiplier for the displacement increment at every time step. The mean of the random multiplier is set to a value that is less than zero, resulting in the restoring force lagging the command displacement and reproduces the effect of systematic time delay [22]. For the simulation, the "Simulated error" block is tuned to produce a 4 ms time delay. Figure 6b summarises the details of this process.

Two recorded earthquake ground motion records are used in these simulations, from the 1978 Tabas earthquake (Iran) and 1995 Kobe earthquake (Japan). The records of both earthquakes are shown in Figure 7.

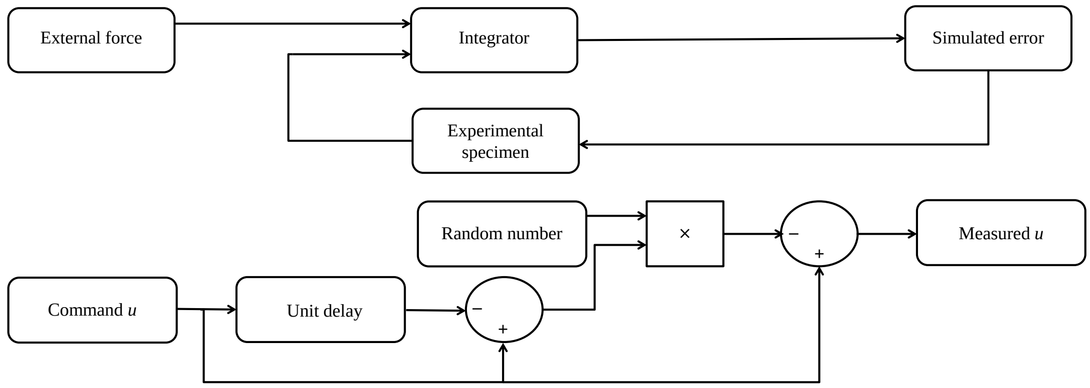

a)

b)

Figure 6: ***a) Complete block diagram of a numerical simulation of a PSD test, and b) simulation of systematic undershooting error inside the "Systematic error" block.***

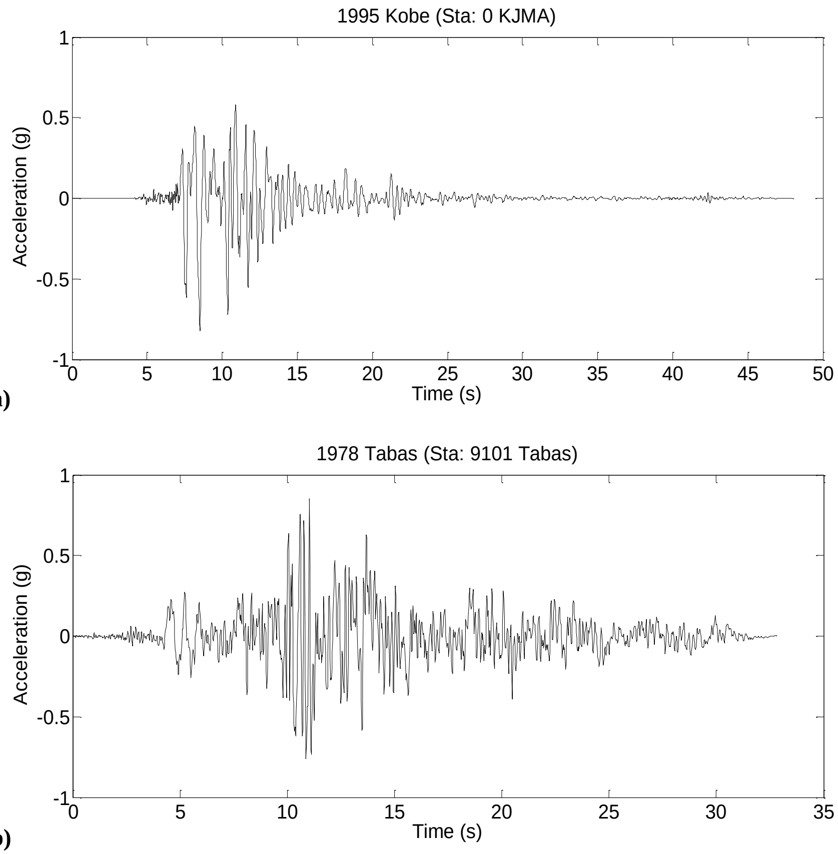

a)

b)

Figure 7: ***Ground acceleration records, a) 1995 Kobe (Sta: 0 KJMA) and b) 1978 Tabas (Sta: 9101 Tabas).***

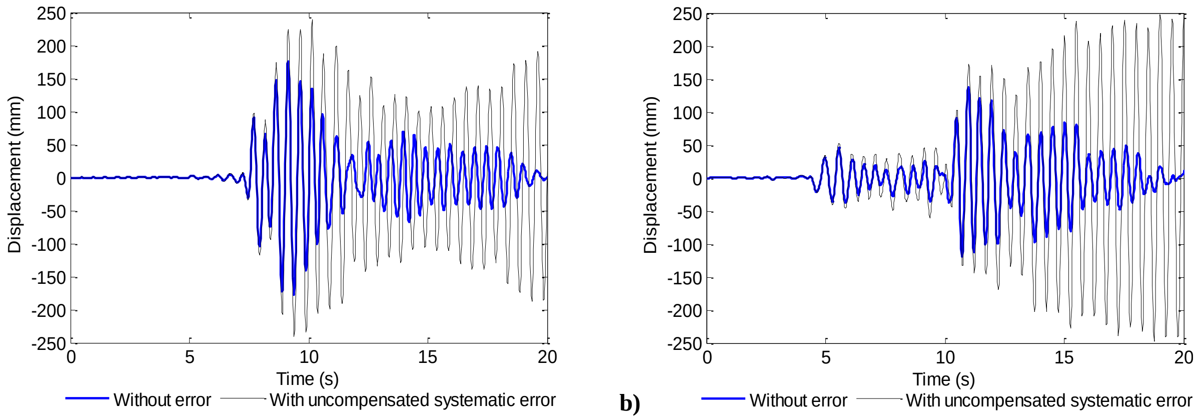

a)

b)

Figure 8: ***Displacement responses without displacement error and with uncompensated systematic displacement error to a) 1995 Kobe earthquake and b) 1978 Tabas earthquake.***

Figures 8a and 8b show the displacement responses of the SDOF structure with and without simulated displacement errors subjected to the two earthquakes. The results are shown for the first 20 seconds of each excitation, when instabilities start to occur. These figures clearly show that the simulated actuator lag has resulted in additional energy in the system which is represented by the large erroneous response. This highlights the importance of compensating actuator delay to avoid such instabilities in real experiments.

Figure 9 shows a comparison of cumulative energy error according to the three expressions described in this paper (Equations 6, 7, and 12). The three methods produced similar error magnitudes, however upon closer inspection the energy error calculated from Equation 7 visibly differs from the rest.

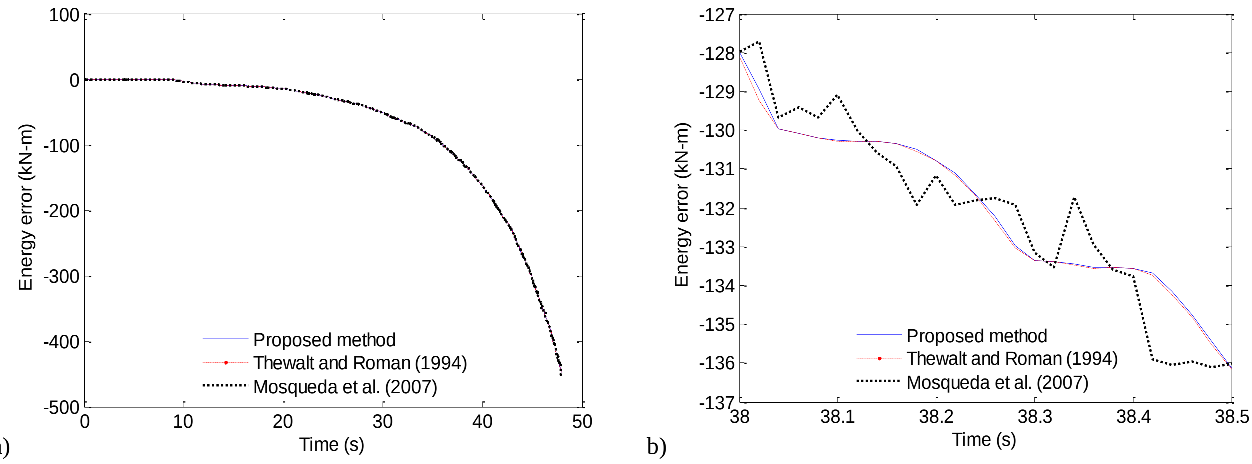

Figure 9: ***Cumulative energy error as calculated using the proposed method, Thewalt and Roman [15], and Mosqueda et al. [16].***

The displacement responses of the structure under the same excitations with the proposed error compensation scheme applied are shown in Figure 10a and 10c for the Kobe and Tabas earthquakes respectively. It can be seen that the corrected responses accurately match the ideal response for both excitations. Figures 10b and 10d show a snapshot of the displacement responses to the Kobe and Tabas earthquakes respectively. These highlight the remaining minor discrepancies between the response with the proposed error compensation and the ideal response. The two main causes of the discrepancies are 1) the energy error used to derive the correcting variable viscous damping (Equation 12) is only an approximation to the energy error represented by Equation 6; and 2) predictor velocity is used in the algorithm instead of the true velocity because of the practicality of implementation.

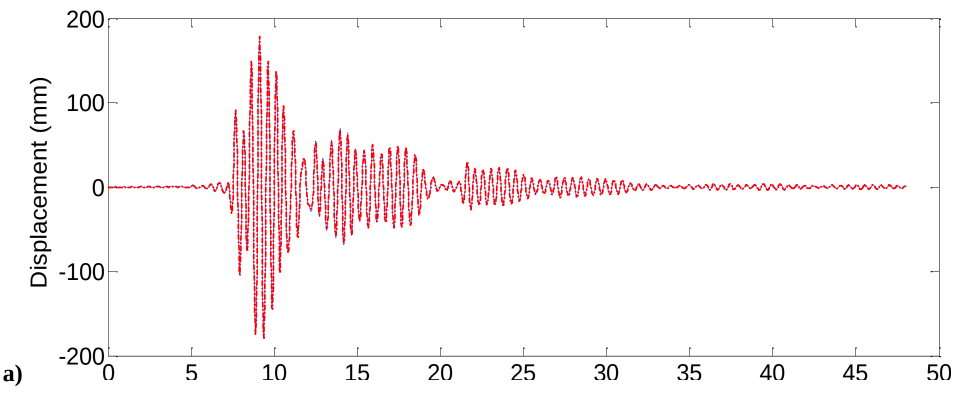

Figure 10: ***Displacement response without displacement error and with compensated systematic displacement error subjected to a) and b) 1995 Kobe earthquake. (Continued on the next page).***

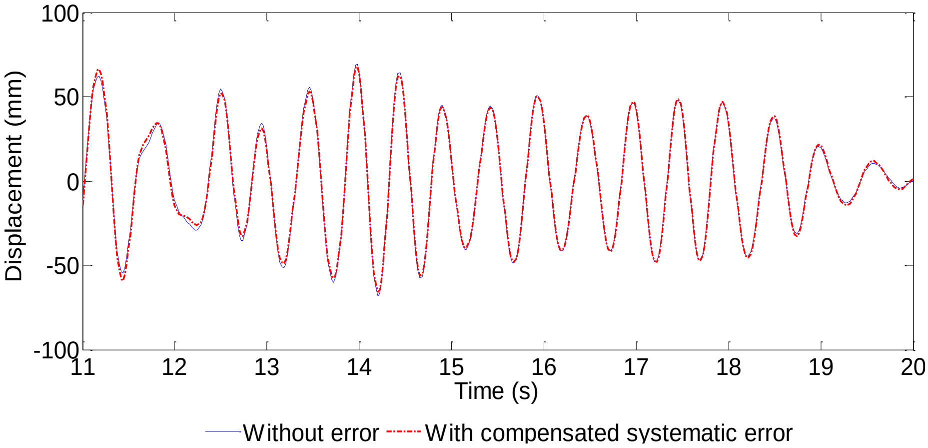

b)

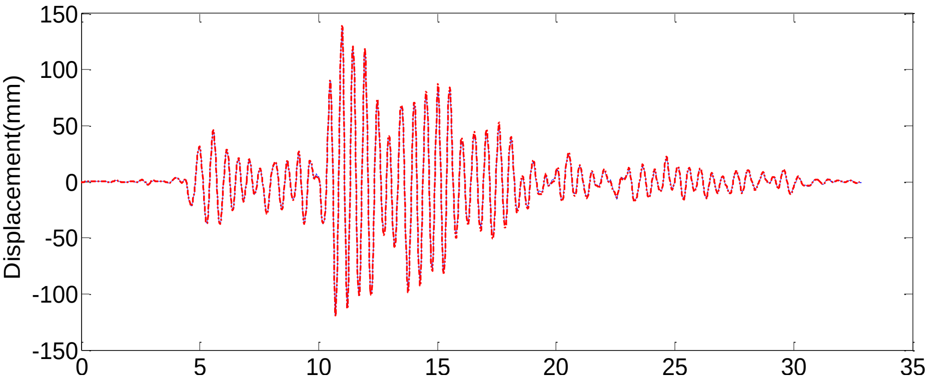

c)

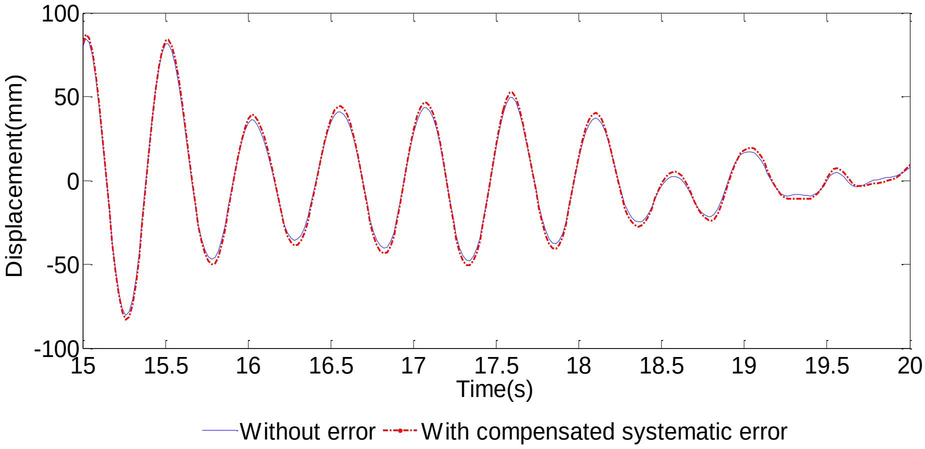

d)

Figure 10 (continued): ***Displacement response without displacement error and with compensated systematic displacement error subjected to a) and b) 1995 Kobe earthquake, c) and d) 1978 Tabas earthquake.***

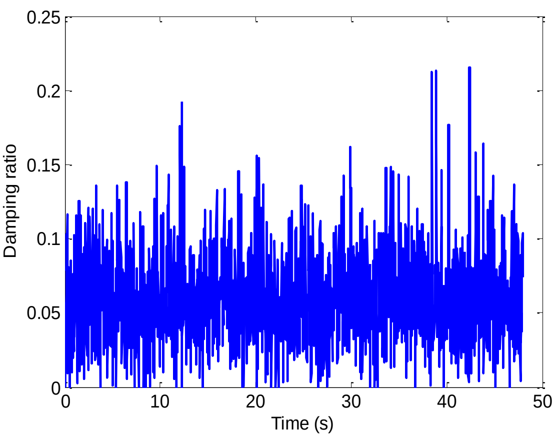

a)

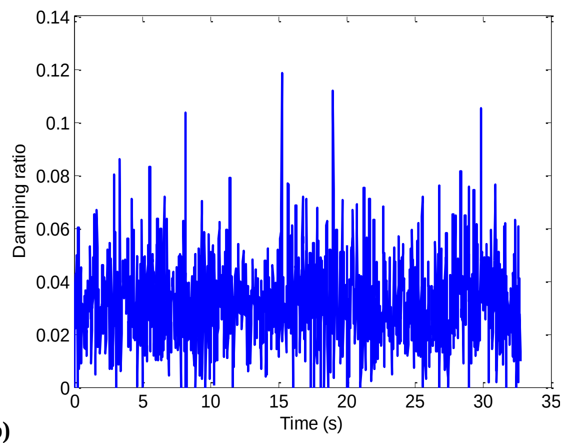

b)

Figure 11: ***Additional variable damping ratio to compensate for energy error in the responses subjected to a) 1995 Kobe earthquake and b) 1978 Tabas earthquake.***

Figure 11 shows the equivalent variable viscous damping ratio introduced into the system to compensate for the energy error at each time step. It can be seen that the amount of artificial viscous damping needed for compensation reached as high as 22% and 12% for the response to the Kobe earthquake (Figure 11a) and Tabas earthquake (Figure 11b) respectively. Considering the inherent viscous damping in typical structures is approximately 5% of critical damping, this confirms that even under a relatively small time delay (4 ms), the negative damping introduced to the system (the opposite of added damping required to compensate for the response) can exceed that available in the system and hence producing the unstable response.

In the calculation of the variable viscous damping presented in Equation 14, a strategy is needed to mitigate the asymptotic mathematical error when the denominator in the Equation 14 becomes very small. This results in a very large amount of viscous damping compensation which can reduce the effectiveness of the proposed scheme. Figure 12 shows the relationships between the energy error and the two bracketed terms in the denominator in Equation 14, the "sum of velocities" and "incremental displacement". For brevity, only the relationships in the response to Kobe earthquake are presented, but similar trend are also observed in the other simulation.

From Figure 12a it can be seen that as the sum of velocities approaches zero from either direction, the energy error also approaches zero. Similar trend can be observed for the incremental displacement presented in Figure 12b, which is expected as incremental displacement is a first order approximation of velocity. Because of this, the sum of velocities and incremental displacements approaches zero simultaneously and explains how Equation 14 results in an erroneously large compensation viscous damping. Exploiting the linear relationship between incremental displacements and sum of velocities as demonstrated by Figure 13, it is proposed that when the denominator in Equation 14 becomes very small (i.e. when the velocity parameters making up the "sum of velocities" term have different sign), the variable viscous damping at the current time step takes the same value as that from the previous time step. This is implemented in the simulation and gave the satisfactory results presented in Figure 10.

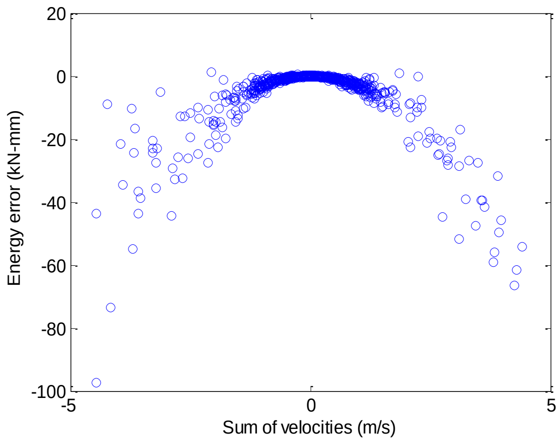

a)

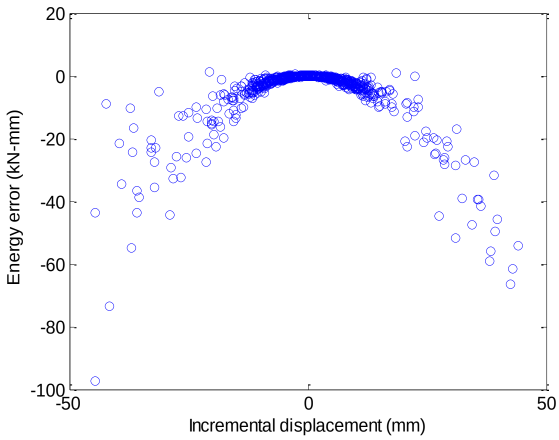

b)

Figure 12: ***Relationship between the energy error and a) the sum of velocities and b) the incremental displacement for the response to Kobe earthquake.***

For completeness, the accuracy of the proposed method is quantified in terms of the normalized maximum error, ε^{max}, and the normalized root-mean-square of error, ε^{rms}, similar to that published in Mosqueda *et al.* [17]. They are expressed as,

$$\varepsilon^{max} = \frac{max|u^{sim} - u^{ideal}|}{max|u^{ideal}|} \tag{17}$$

$$\varepsilon^{rms} = \frac{rms|u^{sim} - u^{ideal}|}{max|u^{ideal}|} \tag{18}$$

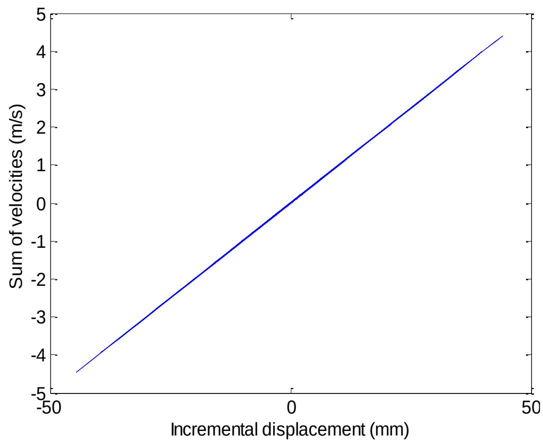

Figure 13: ***Relationship between the sum of velocities and the incremental displacement of the response to 1995 Kobe earthquake.***

In these equations, u^{sim} is the displacement response of the structure from simulation with induced experimental errors, and u^{ideal} is the ideal displacement response from identical simulation without errors. ε^{max} measures the peak error while ε^{rms} provides a measure of the degree of match throughout the simulation. Correspondingly, the ε^{max} and ε^{rms} for the simulation with the Kobe earthquake motion are 0.0349 and 0.007 respectively, and 0.0265 and 0.095 for the Tabas earthquake motion. These relatively small values indicate that the proposed compensation scheme performed well in correcting the response.

EXPERIMENTAL VALIDATION

This section presents the results from a series of experiments validating the proposed compensation scheme. The test specimen is a steel moment resisting frame (MRF) as shown in Figure 14. Concrete blocks with a total mass of 1.158 tons are attached on the steel beam at the top of the frame. The concrete blocks ensure the frame is in the same stress state as the structure in service. The structure is idealised as a SDOF system.

Figure 14: Steel moment resisting frame specimen (MRF) used in the experimental validations.

From a low amplitude cyclic test the elastic stiffness of the frame is determined to be 358.5 kN/m, which yields an elastic natural period of 0.36 seconds. A hydraulic actuator with ± 150 mm stroke and ± 300 kN load capacity applies the displacements at the top of the frame. An actuator characterisation test has found that there is 33.5 milliseconds inherent delay in the actuator response due to actuator dynamics. With due consideration of the time delay and high natural frequency of the test structure, a time scale of 10 is selected for the testing to avoid test instability.

In real experiments, measurements from force and displacement transducers are invariably affected by noise. In cases when the displacement increments are small, such as that arising from the use of small integration time step, it is possible that measurement noises are greater than the actual displacement control errors. As measurement noises are typically randomly distributed [14], this is likely to lead to uncorrelated force and displacement increment readings, which would be misinterpreted as energy error and negate the efficacy of the compensation algorithm. For the measurement sensors used in the experimental validations, there are a 5 mm and 16 kN peak-to-peak displacement and force noise signals, which account for 1.6% and 2.6% of the total range of the actuator LVDT and load cell capacities respectively. These noise levels are large compared to values reported by other researchers and represent additional challenge ([28, 29]). In order to have a reliable estimation of energy error, the noise level in displacement and restoring force measurements must be reduced. This can be achieved by implementing signal-smoothing procedure such as applying digital lowpass filter on both the displacement and force measurements. However, conventional filtering introduces unavoidable time delay in the filtered response and further increase the time delay from actuator dynamics alone. Thus, it is decided that this kind of filtering is not desirable for the experimental validation as it can lead to test instability. Instead, a Kalman filter is chosen to filter the measured displacement and force response, as it does not introduce phase lag to the filtered quantities. A detailed discussion on the use of Kalman filter can be found in a report by Carrion and Spencer [29].

The effect of noise is particularly important in fast or continuous PSDs where the equations of motion of the test specimens are solved at very high sampling rate. In the experimental validations, the equations of motion are solved and command displacements are sent to the actuator at 2,000 Hz. At this rate, the commanded displacement increment at each time step are likely to be very small thus amplifying the effect of noise.

Systematic displacement control errors have direction and magnitude proportional to the displacement increments [15]. Consequently, the amount of energy error introduced at a given time step is dependant on the magnitude of incremental displacement. This relationship can be observed from Figure 12, where approaching peak displacement, indicated by small velocities or small displacement increment, the magnitudes of energy errors are close to zero representing small displacement errors. So while at these small displacement increments there is little energy error due to actuator delay, the presence of noise or uncorrelated force and displacement readings would mislead the delay compensation algorithm to believe there is large energy error requiring correction.

To overcome this, an additional gain multiplier is added to the numerator of Equation 14. The gain multiplier deactivates the compensation when the incremental displacement is small, and becomes as close as unity as possible when the incremental displacement is within the normal operating range. Therefore the gain multiplier can be viewed as an “ON/OFF" switch which controls the appropriate timing for the compensation scheme to work.

A hyperbolic secant function of the ratio between the displacement and velocity of the structure is found to satisfy these requirements. This form of the gain multiplier is analogous to the velocity gain constant used in delay estimation procedure proposed by Darby *et al.* [20] and is defined as

$$G_{v_i} = \left(\operatorname{sech}\left(\frac{\omega_n u_i}{\dot{u}_{i-1}}\right)\right)^{\gamma} \tag{19}$$

The parameter γ should be selected as $0 < \gamma \leq 1$, this controls the transition steepness between of G_{v_i}. For the experimental validations, γ is selected to be 0.05.

The complete expression for the modified additional variable damping matrix becomes,

$$\boldsymbol{C}_i^{cor} = \frac{-2\boldsymbol{E}_i^{er} G_{v_i}}{(\dot{u}_{i-1} + \dot{\tilde{u}}_i)(u_i^c + u_{i-1}^c)} \tag{20}$$

Both earthquake records used previously in the numerical simulation are also used for the experimental validation. To keep the specimen within the elastic range such that testing can be done for another set of experiments, the ground motion amplitudes are scaled such that the displacement responses of the frame will not exceed 6 mm. Figure 15a and 15c shows the displacement response of the steel frame subjected to Tabas and Kobe earthquake records respectively. Figure 15b and 15d provides a closer view of 15a and 15b for certain time windows. Figure 16 illustrates the “ON/OFF” switching behaviour of G_{v_i} for Tabas excitation. This highlights that not all energy error is corrected at every time step due to the smooth transition of G_v. Therefore, it is important that the parameter γ is tuned so that is G_{v_i}as steep as possible to balance the effects of noise and accurate actuator delay compensation.

This effect of measurement noise can be clearly observed at the beginning of the test in Figure 15a when the excitation amplitudes are very small. During this time when the expected displacements are small, the simulation produces erroneous displacement due to erroneous damping effect from the spurious energy error.

a)

b)

c)

d)

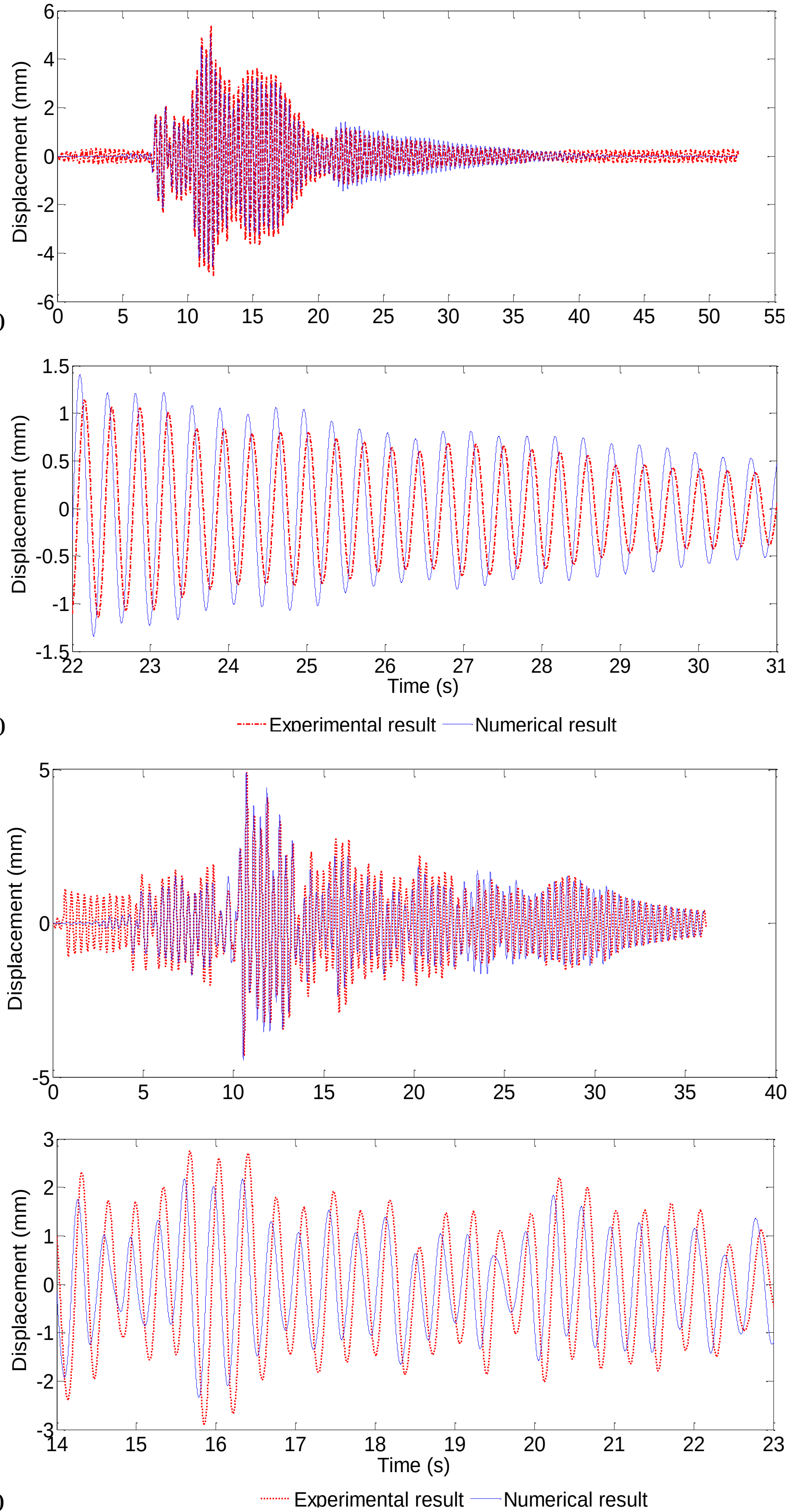

Figure 15: ***Displacement response of the MRF specimen subjected to a) and b) 1995 Kobe earthquake, c) and d) 1978 Tabas earthquake.***

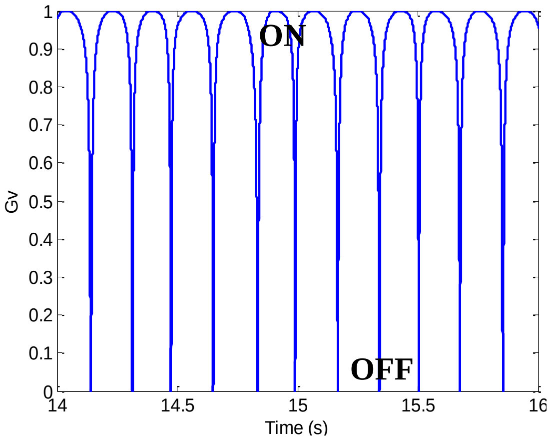

Figure 16: ***G_v in displacement response due to 1995 Kobe earthquake excitation.***

CONCLUSION

This paper presents a new intuitive method to compensate for actuator delay during a fast PSD test. The proposed compensation scheme dissipates the erroneously introduced energy through a varying viscous damping matrix that is proportional to the energy error at each time step. Numerical simulations and experimental validation have been presented to demonstrate the effectiveness of the proposed compensation algorithm to recover the ideal structural response. The experimental validation also highlight the necessity of a gain factor to deactivate the delay compensation scheme at small displacement increments to avoid the scheme wrongly correcting measurement noises. The final proposed compensation algorithm is shown to be simple to apply, requires only data at each current time step of a PSD test, and intuitive as it communicates the error as widely understood viscous damping equivalent.

ACKNOWLEDGMENT

The authors wish to thank the Earthquake Commission for the financial support of this project through the Biennial Research Funding Programme, project BIE12/632.

REFERENCES

[1] Mahin, S.A., P.B. Shing. Pseudodynamic method for seismic testing. *Journal of Structural Engineering,* **111** (7), 1482-503, 1985.

[2] Shing, P.B., S.A. Mahin. Pseudodynamic test method for seismic performance evaluation: theory and implementation. *Report No*. *UCB/EERC-84/01* (University of California, Berkeley, California, 1984).

[3] Takanashi, K., M. Nakashima. Japanese activities on on-line testing. *Journal of Engineering Mechanics,* **113**, 1014, 1987.

[4] Haussmann, G. Evaluation of openfresco and simcor for fast hybrid single site simulation. *Report No*. *CU-NEES-07-2* (University of Colorado, Boulder, Colorado, 2007).

[5] Nakashima, M., H. Kato, E. Takaoka. Development of real-time pseudodynamic testing. *Earthquake Engineering and Structural Dynamics,* **21** (1), 79-92, 1992.

[6] Shing, P.B., Z. Wei, R.Y. Jung, E. Stauffer, NEES fast hybrid test system at the University of Colorado. *Proceedings of the 13th World Conference on Earthquake Engineering*, Vancouver, BC, Canada, 2004

[7] Nakashima, M., N. Masaoka. Real-time on-line test for MDOF systems. *Earthquake Engineering and Structural Dynamics,* **28** (4), 393-420, 1999.

[8] Darby, A.P., A. Blakeborough, M.S. Williams. Real-time substructure tests using hydraulic actuator. *Journal of Engineering Mechanics,* **125** (10), 1133-39, 1999.

[9] Magonette, G. Development and application of large–scale continuous pseudodynamic testing techniques. *Philosophical Transactions of the Royal Society of London. Series A: Mathematical, Physical and Engineering Sciences,* **359** (1786), 1771-99, 2001.

[10] Mercan, O., J.M. Ricles. Stability and accuracy analysis of outer loop dynamics in real-time pseudodynamic testing of SDOF systems. *Earthquake Engineering and Structural Dynamics,* **36** (11), 1523-43, 2007.

[11] Mahin, S.A., P.B. Shing, C.R. Thewalt, R.D. Hanson. Pseudodynamic test method: current status and future directions. *Journal of Structural Engineering,* **115** (8), 2113-28, 1989.

[12] Thewalt, C.R., S.A. Mahin. Hybrid solution techniques for generalized pseudodynamic testing. *Report No. UCB/EERC-87/09* (University Of California, Berkeley, California, 1987).

[13] Mosqueda, G., B. Stojadinović, S.A. Mahin. Implementation and accuracy of continuous hybrid simulation with geographically distributed substructures. *Report No*. *UCB/EERC 2005-02* (University of California, Berkeley, California, 2005).

[14] Shing, P.B., S.A. Mahin. Experimental error propagation in pseudodynamic testing. *Report No. UCB/EERC-83/12* (University of California, Berkeley, California, 1983).

[15] Thewalt, C.R., M. Roman. Performance parameters for pseudodynamic tests. *Journal of Structural Engineering,* **120** (9), 2768-81, 1994.

[16] Mosqueda, G., B. Stojadinovic, S.A. Mahin. Real-time error monitoring for hybrid simulation. Part I: Methodology and experimental verification. *Journal of Structural Engineering,* **133** (8), 1100-08, 2007.

[17] Mosqueda, G., B. Stojadinovic, S.A. Mahin. Real-time error monitoring for hybrid simulation. Part II: structural response modification due to errors. *Journal of Structural Engineering,* **133** (8), 1109-17, 2007.

[18] Ahmadizadeh, M., G. Mosqueda. Online energy-based error indicator for the assessment of numerical and experimental errors in a hybrid simulation. *Engineering Structures,* **31** (9), 1987-96, 2009.

[19] Horiuchi, T., M. Inoue, T. Konno, Y. Namita. Real-time hybrid experimental system with actuator delay compensation and its application to a piping system with energy absorber. *Earthquake Engineering and Structural Dynamics,* **28** (10), 1121-41, 1999.

[20] Darby, A.P., M.S. Williams, A. Blakeborough. Stability and delay compensation for real-time substructure testing. *Journal of Engineering Mechanics,* **128** (12), 1276-84, 2002.

[21] Carrion, J.E., B. Spencer, Real-time hybrid testing using model-based delay compensation. *Proceedings of the 4th International Conference on Earthquake Engineering,* Taipe, Taiwan, 2006

[22] Ahmadizadeh, M., G. Mosqueda, A. Reinhorn. Compensation of actuator delay and dynamics for real-time hybrid structural simulation. *Earthquake Engineering and Structural Dynamics,* **37** (1), 21-42, 2008.

[23] Zhao, J., C. French, C. Shield, T. Posbergh. Considerations for the development of real-time dynamic testing using servo-hydraulic actuation. *Earthquake Engineering and Structural Dynamics,* **32** (11), 1773-94, 2003.

[24] Bonnet, P., C. Lim, M. Williams, A. Blakeborough, S. Neild, D. Stoten, C. Taylor. Real-time hybrid experiments with Newmark integration, MCSmd outer-loop control and multi-tasking strategies. *Earthquake Engineering and Structural Dynamics,* **36** (1), 119-41, 2007.

[25] Carrion, J.E., B. Spencer, B.M. Phillips. Real-time hybrid simulation for structural control performance assessment. *Earthquake Engineering and Engineering Vibration,* **8** (4), 481-92, 2009.

[26] Wallace, M., D. Wagg, S. Neild. An adaptive polynomial based forward prediction algorithm for multi-actuator real-time dynamic substructuring. *Proceedings of the Royal Society A: Mathematical, Physical and Engineering Science,* **461** (2064), 3807-26, 2005.

[27] Chen, C., J.M. Ricles. Tracking error-based servohydraulic actuator adaptive compensation for real-time hybrid simulation. *Journal of Structural Engineering,* **136** (4), 432-40, 2010.

[28] Mosqueda, G. Continuous hybrid simulation with geographically distributed substructures. University of California Berkeley, California (2003).

[29] Carrion, J.E., B. Spencer. Model-based Strategies for Real-time Hybrid Testing. *Report No. UILU-ENG-2007-1806* (University of Illinois at Urbana-Champaign, 2007).